DALTON
FULL PAPER

Extended one- and two-dimensional copper(II) complexes with bridging (N–N) diazine ligands: structural and magnetic studies †

Zhiqiang Xu,[a] Stephen White,[a] Laurence K. Thompson,*[a] D. O. Miller,[a] Masaaki Ohba,[b] Hisashi Ōkawa,[b] Claire Wilson[c] and Judith A. K. Howard[c]

[a] *Department of Chemistry, Memorial University, St. John's, Newfoundland, A1B 3X7, Canada. E-mail: lthomp@morgan.ucs.mun.ca*
[b] *Department of Chemistry, Faculty of Science, Kyushu University, Hakozaki, Higashi-Ku, Fukuoka 812-8581, Japan*
[c] *Department of Chemistry, University of Durham, Durham, UK DH1 3LE*

Received 14th December 1999, Accepted 10th April 2000
Published on the Web 11th May 2000

One- and two-dimensional copper(II) complexes of the polydentate diazine ligands pahap and pypz are reported, in which two copper(II) centers are bridged by a rotationally flexible single N–N bridge in a basic dinuclear subunit, with these subunits linked by halogen atom bridges to provide extended chains and layers. Crystal structures are reported for $[Cu_2(pypz)Cl_4]\cdot H_2O$ (**1**), $[Cu_2(pypz)Br_4]\cdot H_2O$ (**2**) and $[Cu_2(pahap)Cl_4]$ (**3**). In **1** and **2** the dinuclear subunits are internally bridged by halogen atoms to form tetranuclear dimers, which then link to form a two-dimensional chicken wire lattice. The dinuclear subunits exhibit intra-molecular ferromagnetic coupling, associated with acute angles of rotation of the copper magnetic planes around the N–N single bond bridge, in complete agreement with previous magneto-structural results. However, low temperature phase transitions (<15 K) indicate the presence of significant antiferromagnetic components, which are associated with spin pairing between adjacent ferromagnetic layers. In addition long range, weak ferromagnetic ordering is observed below 5 K, and confirmed by magnetic hysteresis measurements. The complicated magnetic data have been interpreted in terms of a model involving one-dimensional ferromagnetic chains arranged in two-dimensional layers, with the layers linked antiferromagnetically, leading to metamagnetic behaviour, with additional interchain ferromagnetic coupling appearing at low temperatures. Compound **3** has a much larger rotational angle of the copper magnetic planes around the N–N bond (120.3°), and a different extended structure involving a linear chain of chlorine atom bridged tetranuclear subunits. The magnetic properties of **3** are interpreted using an alternating chain model, and are dominated by intramolecular antiferromagnetic exchange between copper(II) centers within each dinuclear subunit.

Introduction

The diazine (N_2) moiety in heterocyclic ring systems is rigidly fixed, while the N–N diazine linkages in open-chain systems containing N–N single bonds are much more flexible,[1] leading to several possible mononucleating and dinucleating coordination modes.[2–6] Polyfunctional open-chain diazine ligands have been shown to form mononuclear,[6–9] dinuclear,[10–16] and even trinuclear[17] and tetranuclear copper(II) complexes.[18,19]

Recent studies[20–22] on dicopper(II) complexes of a series of novel bis-bidentate open-chain diazine ligands (*e.g.* pahap, pypz) have shown that the two copper(II) centers are bridged by the diazine N–N single bond, and have a great deal of rotational flexibility depending on co-ligands, steric interactions and hydrogen bonding associations. Rotational angles between the copper magnetic planes occur over a 105° range, with a particular conformation resulting from these secondary constraints. A linear relationship has been found between the magnetic plane rotation angle and the exchange integral, with a change from ferromagnetic coupling at angles <80° to antiferromagnetic coupling >80°.[20–22]

The present study describes three new complexes with rotational flexibility around the N–N single bond, which is limited in two cases by weak axial halogen atom (Cl, Br) bridging interactions, leading to small angles between the copper magnetic planes. Further bridging interactions in these systems

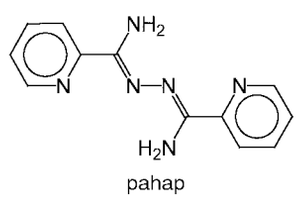

pahap

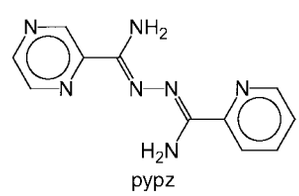

pypz

lead to the formation of extended, irregular one-dimensional chains, which associate into two-dimensional lattice structures with 'chicken-wire' layered arrangements. Ferromagnetic coupling prevails within each dinuclear subunit and within the chains and layers leading to weak long range ferromagnetic ordering at low temperature, but a significant additional extended inter-layer antiferromagnetic interaction dominates the low temperature magnetic behavior. The third complex has no intra-molecular bridging constraint, and the dinuclear structure relaxes with a larger inter-plane angle. Further halogen bridging interactions lead to association of the dinuclear subunits into a linear chain structure. The magnetic properties are interpreted using an alternating one-dimensional chain model,

† Dedicated to the memory of Professor Olivier Kahn.

DOI: 10.1039/a909824k

Table 1 Summary of crystallographic data for **1**–**3**

Compound	**1**	**2**	**3**
Empirical formula	$C_{11}H_{13}Cu_2N_7Cl_4O$	$C_{11}H_{13}Cu_2N_7Br_4O$	$C_{12}H_{12}Cu_2N_6Cl_4$
M	528.17	705.98	509.16
Crystal system	Monoclinic	Monoclinic	Monoclinic
Space group	*C*2/*c*	*C*2/*c*	*C*2/*c*
a/Å	26.754(3)	27.260(4)	15.1717(4)
b/Å	8.466(3)	8.688(8)	8.3275(2)
c/Å	16.334(3)	16.644(5)	15.2603(4)
α/°	90	90	90
β/°	100.94(1)	100.45(2)	116.037(1)
γ/°	90	90	90
U/Å^3	3632(1)	3876(3)	1732.46(8)
ρ_{calc}/g cm^{-3}	1.931	2.419	1.952
T/K	299(1)	299(1)	120(1)
Z	8	8	4
μ/mm^{-1}	8.458	10.48	3.079
Reflections collected: total, independent, R_{int}	3004, 2930, 0.055	4873, 4773, 0.055	10640, 2425, 0.0267
Final *R*, R_w	0.058, 0.039	0.049, 0.048	0.0185(R_1), 0.0464(wR_2)

dominated by intra-molecular antiferromagnetic coupling, typical of such systems.

Experimental

Materials

Commercially available solvents and chemicals were used without further purification.

Physical measurements

Melting points were measured on a Fisher-Johns melting point apparatus. Electronic spectra were recorded as Nujol mulls and in solution using a Cary 5E spectrometer. Infrared spectra were recorded as Nujol mulls using a Mattson Polaris FT-IR instrument. Mass spectra were obtained using a VG micromass 7070HS spectrometer. C, H, N analyses on vacuum dried samples (24 h) were performed by the Canadian Microanalytical Service, Delta, B.C., Canada. Variable temperature and variable field magnetic data (2–300 K) were obtained with a Quantum Design MPMS5S Squid magnetometer. Calibrations were carried out with $HgCo(NCS)_4$ and a palladium standard cylinder, and temperature errors were assessed with $[TMENH_2][CuCl_4]$ ($TMENH_2 = (CH_3)_2HNCH_2CH_2NH(CH_3)_2^{2+}$).[23]

Preparations

Ligands. Pahap was prepared according to a published procedure.[20,21] Pypz was made in a similar fashion to that used for pahap,[20,21] using 2-pyrazinamide hydrazone instead of picolinamide hydrazone, with a 90% yield (mp 212–214 °C) (Found: C, 54.97; H, 4.53; N, 41.19. $C_{11}H_{11}N_7$ requires C, 54.77; H, 4.60; N, 40.67%). Mass spectrum (major mass peak; *m*/*z*): 241 (M), 225, 224 (M − NH_2), 196, 195, 163, 162, 121, 120, 106, 105, 80, 79. ν_{max}/cm^{-1} 1606 (C=N), 3408, 3301 (NH).

Complexes. *[Cu_2(pypz)Cl_4]·H_2O* (**1**). Pypz (0.24 g, 1.0 mmol) was added to an aqueous solution of $CuCl_2{\cdot}2H_2O$ (0.68 g, 4.0 mmol) in water (20 mL), and the mixture stirred for several minutes at room temperature until the ligand dissolved. The deep green solution was filtered and the filtrate allowed to stand at room temperature for several days. Dark green diamond shaped crystals formed, which were suitable for structural analysis. These were filtered off, washed with cold de-ionized water and air dried (yield 80%) (Found: C, 24.67; H, 2.48; N, 18.20. $[Cu_2(C_{11}H_{11}N_7)Cl_4]{\cdot}H_2O$ requires C, 25.00; H, 2.48; N, 18.56%).

[Cu_2(pypz)Br_4]·H_2O (**2**). This compound was prepared in a similar manner to **1** using $CuBr_2$, and obtained as khaki brown crystals suitable for structural analysis (yield 75%) (Found: C, 18.94; H, 1.83; N, 14.07. $[Cu_2(C_{11}H_{11}N_7)Br_4]{\cdot}H_2O$ requires C, 18.71; H, 1.86; N, 13.88%).

[Cu_2(pahap)Cl_4] (**3**). Pahap (1.46 g, 6.00 mmol) was added to an aqueous solution of $CuCl_2{\cdot}2H_2O$ (4.0 g, 24 mmol) (150 mL), and the mixture stirred at room temperature until the ligand dissolved. The deep green solution was filtered after 24 h and the filtrate allowed to stand at room temperature for several days. Dark green crystals formed, which were suitable for structural analysis. These were filtered off, washed with cold water and air dried (yield 1.6 g, 51%) (Found: C, 28.37; H, 2.38; N, 16.57. $[Cu_2(C_{12}H_{12}N_6)Cl_4]$ requires C, 28.31; H, 2.37; N, 16.50%).

Crystallography

$[Cu_2(pypz)Cl_4]{\cdot}H_2O$ (1), $[Cu_2(pypz)Br_4]{\cdot}H_2O$ (2). The diffraction intensities of a dark green, irregular crystal of **1** were collected with graphite-monochromatized Cu-Kα X-radiation using a Rigaku AFC6S diffractometer at 299(1) K and the ω–2θ scan technique. The data were corrected for Lorentz and polarization effects. The structure was solved by direct methods.[24,25] All atoms except hydrogens were refined anisotropically. Hydrogen atoms were placed in calculated positions. Neutral atom scattering factors[26] and anomalous-dispersion terms[27,28] were taken from the usual sources. All calculations were performed with the teXsan[29] crystallographic software package using a PC computer. Crystal data collection and structure refinement for **2** were carried out in a similar manner. Abbreviated crystal data for **1** and **2** are given in Table 1.

$[Cu_2(PAHAP)Cl_4]$ (3). Data collection for a dark green crystal of **3** was made using graphite-monochromated Mo-Kα X-radiation with a Bruker SMART CCD detector diffractometer equipped with a Cryostream N_2 flow cooling device.[30] Unit cell parameters were determined and refined with the SMART software,[31a] raw frame data were integrated using the SAINT programme,[31b] and the structure was solved using direct methods and refined by full-matrix least squares on F^2 using SHELXTL.[32] Hydrogen atom positions were located in difference Fourier syntheses. All atoms except hydrogen were refined anisotropically. Abbreviated crystallographic data for **3** are summarized in Table 1.

CCDC reference number 186/1935.

See http://www.rsc.org/suppdata/dt/a9/a909824k/ for crystallographic files in .cif format.

Results and discussion

Synthetic procedures

Reaction conditions for the synthesis of **3** differ slightly from

Table 2 Selected bond distances (Å) and angles (°) for **1**

Cu(1)–Cl(1)	2.243(2)	Cu(2)–Cl(4)	2.238(1)
Cu(1)–Cl(2)	2.263(1)	Cu(2)–N(4)	1.977(3)
Cu(1)–N(1)	2.033(3)	Cu(2)–N(6)	2.040(4)
Cu(1)–N(2)	1.996(3)	N(2)–N(4)	1.426(4)
Cu(2)–Cl(3)	2.243(1)	Cu(1)–Cu(2)	3.831(1)
Cl(1)–Cu(1)–Cl(2)	94.19(5)	Cl(3)–Cu(2)–Cl(4)	93.94(5)
Cl(1)–Cu(1)–N(1)	93.3(1)	Cl(3)–Cu(2)–N(4)	93.3(1)
Cl(1)–Cu(1)–N(2)	168.9(1)	Cl(3)–Cu(2)–N(6)	166.65(9)
Cl(2)–Cu(1)–N(1)	171.0(1)	Cl(4)–Cu(2)–N(4)	172.1(1)
Cl(2)–Cu(1)–N(2)	93.9(1)	Cl(4)–Cu(2)–N(6)	93.2(1)
N(1)–Cu(1)–N(2)	79.4(1)	N(4)–Cu(2)–N(6)	80.2(1)

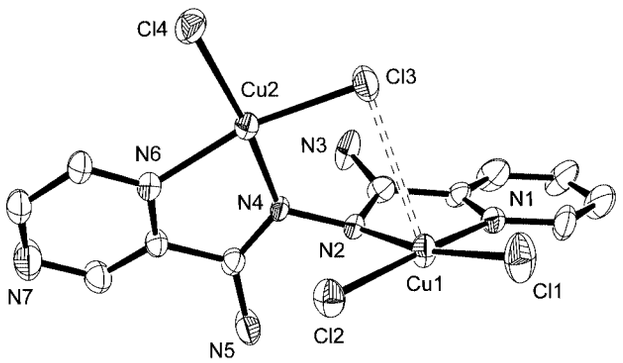

Fig. 1 Structural representation of the dinuclear subunit in $[Cu_2(pypz)Cl_4]\cdot H_2O$ (**1**) with hydrogen atoms omitted (40% probability thermal ellipsoids).

those used to produce the parent complex $[Cu_2(pahap)Cl_4]\cdot H_2O$.[20] In this case the reaction between pahap and $CuCl_2\cdot 2H_2O$ was carried out in water with a 2 : 1 metal to ligand ratio, while for **3** a 4 : 1 ratio was used. Anhydrous analogues of **1** and **2** have not yet been synthesized.

Structures

Crystal structure of $[Cu_2(pypz)Cl_4]\cdot H_2O$ (1). The structure of the dinuclear fragment of **1** is illustrated in Fig. 1, and bond distances and angles relevant to the copper coordination spheres are listed in Table 2. The complex has a twisted dinuclear structure with the copper(II) basal planes rotated around the N–N single bond (N(2)–N(4) 1.426(4) Å) at an acute angle. This occurs mainly as a result of a weak axial interaction between Cu(1) and Cl(3) (Fig. 1; Cu(1)···Cl(3) 3.111(2) Å), which fixes the molecular conformation of the complex and leads to a copper–copper separation of 3.831(1) Å. Within each dinuclear subunit the copper basal least-squares planes (CuN_2Cl_2) are twisted by 69.4°, while the CuN_2C_2 chelate ring least-squares planes are twisted by 77.0°, with a Cu(1)–N(2)–N(4)–Cu(2) torsional angle of 54.9°. Axial contacts of 2.981(2) Å between Cu(2) and Cl(4) link two dinuclear units into an associated tetranuclear linear chain (Fig. 2; fragment Cu(1)–Cu(2)–Cu(2)–Cu(1); donor atoms only included), making the copper centers all square-pyramidal. The Cu(2)···Cu(2)′ separation (3.691(2) Å) is somewhat smaller than the intra-dinuclear separation (3.831(1) Å), due to the double chloro-bridge.

The lattice structure reveals that there are additional weak but significant single chlorine atom bridging contacts (Cu(1)–Cl(1)′ 3.199(2) Å), which link the tetranuclear subunits into a complex two-dimensional *chicken wire* lattice, which propagates in the *b* direction along a diagonal of the *ac* plane. A fragment of the layer is shown in Fig. 2 (pyridine ring carbons and NH_2 groups removed for clarity). The Cu(1)···Cu(1)′ separation (5.329(2) Å) is quite long as a result of the single chlorine atom bridge. In the two-dimensional layer the repeating unit in the array is a 10-membered metallocyclic ring (Fig. 2), which

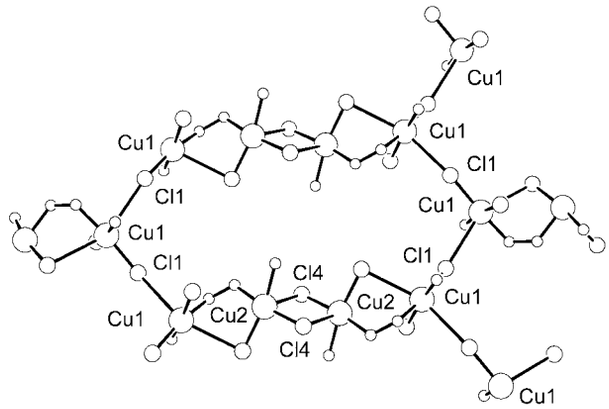

Fig. 2 Structural representation of a segment of the two-dimensional layer structure in **1**.

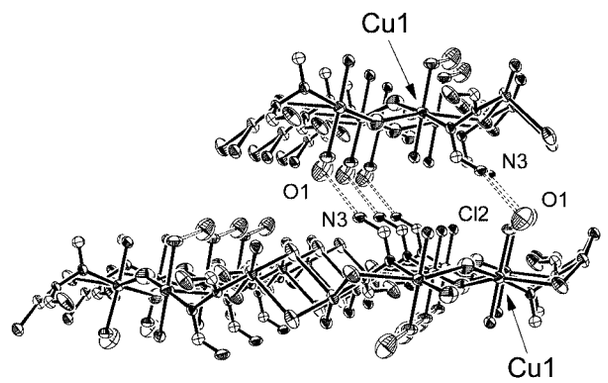

Fig. 3 Layer projection of **1** showing some interlayer contacts.

includes four Cu(2) centers, and six Cu(1) centers, and involves two tetranuclear subunits linked at their ends by the axial Cu(1)–Cl(1) interactions. The layer structure can also be envisaged as a sequence of loosely connected *zig-zag* chains, connected orthogonally *via* Cu(1)–Cl(1) bridges. Interlayer contacts involving halogen–halogen interactions are very weak (*e.g.* nearest Cl···Cl contact 4.722 Å; sum of van der Waals contacts 3.6 Å), and so cannot be considered significant in terms of a possible interlayer pathway for magnetic exchange (*vide infra*). Stacking contacts between the pyridine rings are quite significant (*e.g.* minimum contact distance 3.429 Å), and while they possibly affect the way in which the layers pack, they cannot be considered viable magnetic exchange pathways either.

The role of the water molecule (O(1)) in the structure appears to be quite important, not only from the viewpoint of the conformation of the dinuclear center itself, but also the overall structure. Four contacts involving O(1) within 3.5 Å include N(5) (2.939 Å), N(3) (3.305 Å), Cl(1) (3.430 Å) and Cl(2) (3.425 Å), all of which might influence the orientation of the copper planes within the dinuclear subunits, and also the associated subunits, but more importantly the interlayer associations. The contacts involving N(5), N(3), Cl(1) and Cl(2) link the layers together producing what is effectively a three dimensional structural arrangement. Fig. 3 illustrates one such connection involving N(3) and Cl(2), which generates a six bond connecting pathway between the metals, linking them equatorially. Others leading to similar equatorial connections include Cu(1)–Cl(1)–O(1)–N(3)–C(6)–N(2)–Cu(1) and Cu(2)–N(4)–C(7)–N(5)–O(1)–N(3)–C(6)–N(2)–Cu(1). These connections link every second copper in each chain across the layers thus producing a large number of links, all having the potential to provide a possible spin exchange route between the layers.

Crystal structure of $[Cu_2(pypz)Br_4]\cdot H_2O$ (2). The structure of **2** is almost identical to that of **1**, and the tetranuclear subunit structure is illustrated in Fig. 4. Important bond distances and

Table 3 Selected bond distances (Å) and angles (°) for **2**

Br(1)–Cu(1)	2.389(2)	Cu(1)–N(3)	1.994(7)
Br(2)–Cu(1)	2.402(2)	Cu(2)–N(4)	1.996(8)
Br(3)–Cu(2)	2.384(2)	Cu(2)–N(7)	2.018(9)
Br(4)–Cu(2)	2.374(2)	Cu(1)–Cu(2)	3.819(3)
Cu(1)–N(1)	2.028(8)	N(3)–N(4)	1.411(9)
Br(1)–Cu(1)–Br(2)	93.42(6)	Br(3)–Cu(2)–Br(4)	92.10(8)
Br(1)–Cu(1)–N(1)	93.6(2)	Br(3)–Cu(2)–N(4)	94.0(2)
Br(1)–Cu(1)–N(3)	170.0(2)	Br(3)–Cu(2)–N(7)	168.2(2)
Br(2)–Cu(1)–N(1)	170.2(3)	Br(4)–Cu(2)–N(4)	173.8(2)
Br(2)–Cu(1)–N(3)	93.6(2)	Br(4)–Cu(2)–N(7)	94.3(2)
N(1)–Cu(1)–N(3)	80.3(3)	N(4)–Cu(2)–N(7)	79.8(3)

Table 4 Selected bond distances (Å) and angles (°) for **3**

Cu(1)–Cl(1)	2.2493(4)	Cu(1)–N(3)	2.0216(11)
Cu(1)–Cl(2)	2.2882(3)	Cu(1)–Cl(2b)	2.7938(4)
Cu(1)–N(1)	2.0146(13)	N(3)–N(3a)	1.4125(14)
Cl(1)–Cu(1)–Cl(2)	92.05(1)	Cl(2)–Cu(1)–Cl(2b)	85.15(1)
Cl(1)–Cu(1)–N(1)	161.19(4)	N(1)–Cu(1)–N(3)	80.11(5)
Cl(1)–Cu(1)–N(3)	94.53(3)	Cl(2b)–Cu(1)–N(1)	92.80(3)
Cl(1)–Cu(1)–Cl(2b)	105.53(1)	Cl(2b)–Cu(1)–N(3)	92.87(3)
Cl(2)–Cu(1)–N(1)	93.70(3)	Cu(1)–Cl(2)–Cu(1b)	94.85(1)
Cl(2)–Cu(1)–N(3)	173.42(3)		

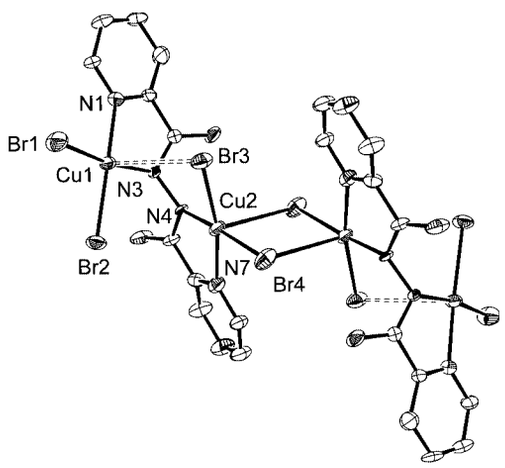

Fig. 4 Structural representation of the tetranuclear subunit in $[Cu_2(pypz)Br_4]\cdot H_2O$ (**2**) with hydrogen atoms omitted (40% probability thermal ellipsoids).

angles are listed in Table 3. Complex **2** has a twisted dinuclear center and a dihedral angle between the CuN_2C_2 planes of 78.4°, with the twist fixed around the single N–N bond (N(3)–N(4) 1.411(9) Å) by a weak axial contact between Cu(1) and Br(3) (3.129(4) Å). The Cu(1)···Cu(2) and Cu(2)···Cu(2)′ separations are 3.819(3) Å and 3.839(2) Å respectively**.** Further associations lead to an extended structural network with inter-tetranuclear linkages between Cu(1) and Br(1) on neighboring molecules (Cu(1)···Br(1)′ 3.286(4) Å; Cu(1)···Cu(1)′ 5.547(4) Å) producing a two-dimensional 'chicken wire' layered array, which is essentially the same as that in **1**. The layers are again linked by significant contacts to O(1) in the same manner as in **1**.

Crystal structure of $[Cu_2(pahap)Cl_4]$ (3). The structure of the dinuclear fragment in **3** is illustrated in Fig. 5, and important bond distances and angle are listed in Table 4. In contrast to the dinuclear centers in **1** and **2**, the structure of **3** is quite different with a relaxation of intra-dinuclear constraints responsible for the acute angles between the copper magnetic planes. The Cu···Cu separation is very long (4.6958(3) Å) as a result of the absence of an intra-dinuclear chlorine atom bridging interaction (Cu(1)···Cl(1) 4.503 Å). This leads to a large Cu–N–N–

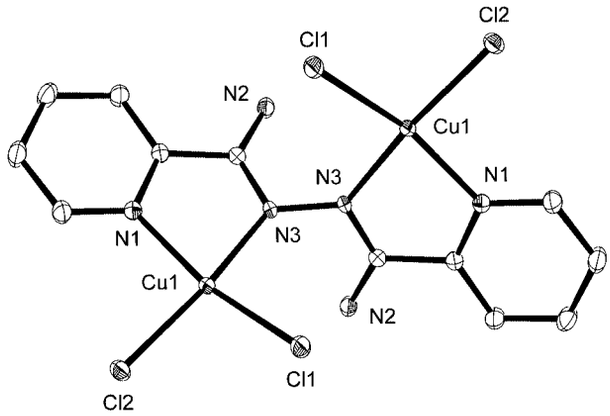

Fig. 5 Structural representation of the dinuclear subunit in $[Cu_2(pahap)Cl_4]$ (**3**) with hydrogen atoms omitted (40% probability thermal ellipsoids).

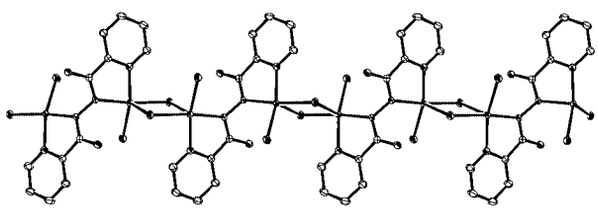

Fig. 6 Extended one-dimensional structural representation of $[Cu_2(pahap)Cl_4]$ (**3**).

Cu torsional angle of 110.3°, and an angle of 120.3° between the CuN_2C_2 chelate rings, which effectively defines the relative orientation of the copper magnetic planes around the N–N bond. Given the general similarity in the structures of the three complexes, and in particular the ligands, the difference between the two structural types can be attributed to the absence of the lattice water molecule in **3**. This not only leads to a dramatic change in the dinuclear structure itself, but also to the extended structure. In this case the structure extends itself by a double chlorine atom bridging interaction between the ends of the molecules forming a one-dimensional chain (Cu(1)–Cl(2)′ 2.794 Å) (Fig. 6). This leads to an inter-dinuclear copper–copper separation (3.758 Å), which is substantially shorter than the intra-molecular distance. The copper $d_{x^2-y^2}$ orbitals are linked orthogonally at this connection with a short (equatorial) and a long (axial) contact. The chains are well separated in the lattice, and there are no significant inter-chain contacts.

The structure of **3** also contrasts dramatically with the structure of the parent complex $[Cu_2(pahap)Cl_4]\cdot H_2O$,[20] which, like **1** and **2**, has a lattice water molecule. A close examination of the structure of $[Cu_2(pahap)Cl_4]\cdot H_2O$ reveals a similar extended structural arrangement to that observed in **1** and **2**, with each dinuclear center linked orthogonally by two chlorine atom bridges, and the resulting tetranuclear subunits linked by single chlorine atom bridges to form a two-dimensional lattice of inter-connected deca-metallic rings. However an examination of the extended lattice structure shows that the water molecules do not have any significant contacts that would link the layers together.

Spectroscopy

Infrared bands associated with the NH_2 groups and lattice and coordinated water are observed for these complexes in the range 3560–3200 cm^{-1}. In general two strong $\nu_{C=N}$ bands are observed in each case above 1635 cm^{-1}, much higher in energy than those of the free ligands ($\nu_{C=N}$ 1606 cm^{-1}), and in agreement with the fact that these ligands adopt a twisted conformation in the complexes.[20] The free ligands themselves have flat structures with significant intramolecular conjugation, which is broken

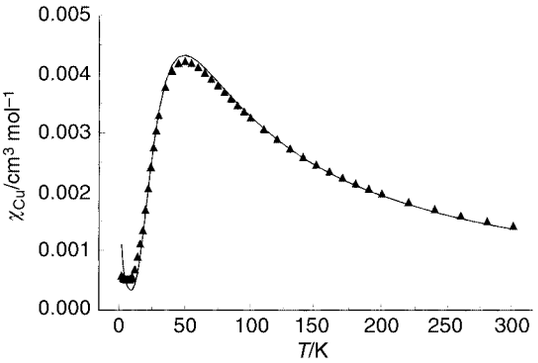

Fig. 7 Variable temperature magnetic data for complex **3**. The solid line was calculated from eqn. (1) with $g = 2.10(1)$, $J_1 = -54.8(4)$ cm^{-1}, $J_2 = 2.2$ cm^{-1}, $\rho = 0.0025$, $N\alpha = 60 \times 10^{-6}$ cm^3 mol^{-1} ($10^2R = 0.6$).

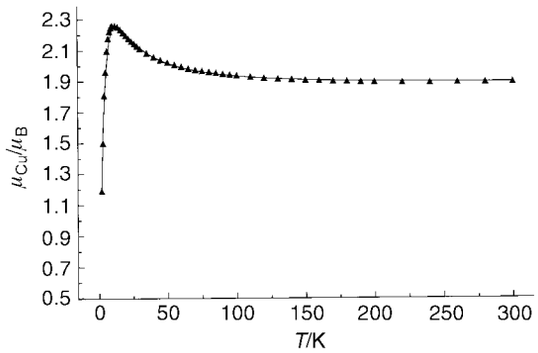

Fig. 8 Variable temperature magnetic data for complex **2**. The solid line (2–300 K) was calculated from eqn. (4), (5) with $g = 2.106(5)$, $J = 9.9(2)$ cm^{-1}, $zJ' = -51.0(5)$ cm^{-1}, $\rho = 0.001$, $N\alpha = 60 \times 10^{-6}$ cm^3 mol^{-1}, ($10^2R = 0.14$).

when the ligands are twisted. Pyridine ring breathing bands are found at 1013 cm^{-1} or higher in all the complexes,[33] in agreement with the fact that all pyridine rings are coordinated. Higher energy bands at 1044 and 1042 cm^{-1} are observed for **1** and **2** respectively, associated with the coordinated pyrazine rings.

Solid state Nujol mull transmittance electronic spectra for **1**–**3** are quite similar, with one broad visible band observed in each case in the range 607–720 nm, consistent with the effective five-coordinate geometries observed at the copper(II) centers. Aqueous solution spectra are slightly different from their solid state spectra, suggesting minor changes to the coordination environment in solution. An aqueous solution of **3** has an identical visible absorption spectrum to that of $[Cu_2(pahap)Cl_4]\cdot H_2O$.[20]

Magnetism

Variable temperature and variable field magnetic susceptibility measurements were carried out on powdered samples of all of the complexes, taken from the same uniform batches used for structural determinations. Complex **3** shows a susceptibility variation with temperature typical of an antiferromagnetically coupled system (Fig. 7) with a maximum in χ_m at ≈50 K. Based on the alternating chain structure of this compound a reasonable magnetic model for **3** would be based on an alternating exchange expression. The short orthogonal, chlorine atom bridged connections between the dinuclear subunits in the chain would be expected to provide weak coupling, and so the overall exchange situation should be dominated by the intra-dinuclear coupling through the N–N bridge. The variable temperature susceptibility data were fitted successfully to a Heisenberg alternating chain expression (based on the Hamiltonian expression in eqn. (1)),[34] with a dominant

$$H = -\sum_{i=1}^{N-1} [J_1 S_{2i}\cdot S_{2i+1} + J_2 S_{2i}\cdot S_{2i-1}] \qquad (1)$$

antiferromagnetic term and a small ferromagnetic term, with $g = 2.10(1)$, $J_1 = -54.8(4)$ cm^{-1}, $J_2 = 2.2$ cm^{-1}, $N\alpha$ (TIP) = 60×10^{-6} cm^3 mol^{-1}, $\rho = 0.0025$ (paramagnetic impurity fraction); $10^2R = 0.6$ ($R = [\Sigma(\chi_{obs} - \chi_{calc})^2/\Sigma\chi_{obs}^2]^{1/2}$). The antiferromagnetic term (J_1) is assigned to the N–N bridge, while the small ferromagnetic term (J_2) is assigned to the orthogonal chlorine atom bridge. The solid line in Fig. 7 was calculated with these parameters. Since $|J_1|$ is so much larger than $|J_2|$ it is not surprising that the data also fit the Bleaney–Bowers equation[35] (eqn. (2))

$$\chi_m = \frac{Ng^2\beta^2}{k(T-\theta)}\left[\frac{1}{(3+\exp(-2J/kT)}\right](1-\rho) + \left(\frac{Ng^2\beta^2}{4kT}\right)\rho + N\alpha \qquad (2)$$

($H = -2JS_1\cdot S_2$; $g = 2.10(1)$, $2J = -56.2(3)$ cm^{-1}, $\theta = 1.2$ K, $\rho = 0.005$, $N\alpha$ (TIP) = 70×10^{-6} cm^3 mol^{-1}, $10^2R = 0.95$). The J values from both fits are comparable and consistent with the predicted behavior of N–N bridged dicopper(II) complexes,[20–22] where antiferromagnetic coupling would be expected with such a large angle between the copper magnetic planes (120.3°). An attempt to fit the data to an alternating antiferromagnetic chain model[36] gave a less satisfactory result.

Room temperature magnetic moments for **1** and **2** are high (1.90 and 1.89 μ_B respectively), and plots of magnetic moment *versus* temperature reveal an increase in moment with decreasing temperature reaching a maximum of 2.14 μ_B at 14 K for **1**, and 2.26 μ_B at 12 K for **2**. In each case the moment then falls dramatically, reaching ≈1.2 μ_B at 2 K in both cases. The plot of μ *versus* temperature for **2** is shown in Fig. 8 (0.1 T field). This behavior is typical of a system which is dominated by ferromagnetic coupling at high temperatures, but has a very significant antiferromagnetic component, which lowers the magnetic moment in the low temperature region. Magnetization measurements were carried out at varying field (0.1 to 5 T) in the temperature range 2–50 K for **1** and **2**. At 2 K magnetic moments remain roughly constant for both **1** and **2** with μ_{Cu} ≈1.2 μ_B for all fields. Raising the temperature to 10 K raises the moment to >2.0 μ_B for all fields, indicating that the antiferromagnetic associations are destroyed. The fact that at 2 K the moment is still 1.2 μ_B at 5.0 T indicates the substantial strength of the antiferromagnetic associations. The plots of χ *versus* temperature for **1** and **2** at 0.1 T reveal an additional feature indicating the presence of strong antiferromagnetic coupling. After a smooth steep rise in χ_{Cu} down to 4.0 K, it then drops sharply at lower temperature.

Fitting of the magnetic data for **1** and **2** to an appropriate exchange equation over the 2–300 K temperature range has proven to be difficult. The structures of both **1** and **2** are composed of connected dinuclear subunits, which quite clearly involve dominant intra-dicopper(II) ferromagnetic exchange.[20–22] The short end-to-end connections of these dinuclear subunits to form tetranuclear subunits, and the subsequent much longer connections of these to form the two-dimensional 'chicken wire' layers, involve orthogonal magnetic connections in all cases, and so would not be expected to generate significant antiferromagnetic exchange. The presence of ferromagnetic exchange through the long subunit connections perhaps seems unlikely, but given the properties of **3**, the short Cu(2)–Cu(2)′ contacts (3.691 Å (**1**), 3.839(2) Å (**2**)) might possibly propagate weak ferromagnetic coupling. However the bulk magnetic properties of **1** and **2** are reasonably associated with some two-dimensional or three-dimensional feature of the structure. The only significant interlayer connections occur *via* O(1) (*vide ante*), and it should be emphasized that they connect copper magnetic orbitals directly, and so could be responsible for long range antiferromagnetic ordering. It should also be

noted that in general the layers are quite close together (*e.g.* Cu(1a)–Cu(1b) 8.23 Å, Cu(2a)–Cu(2b) 6.39 Å, Cu(1a)–Cu(2b) 8.11 Å) and there are numerous linkages between the layers *via* O(1) (Fig. 3).

The Bleaney–Bowers equation (eqn. (2)) can be used to fit the variable temperature data for these complexes, but only if the low temperature data (<14 K) are excluded. It will not account for the drop in μ at low temperature, even with large negative θ values. The large distances separating the ends of the tetranuclear subunits (Cu(1)–Cu(1)′ 5.329 Å (**1**), 5.547 Å (**2**)) might suggest that a chain model would not be realistic. However the magnetic profiles for **2** and **3** bear a close resemblance to a ferromagnetically coupled azide bridged chain compound, which exhibits interchain antiferromagnetic coupling (metamagnet).[37] Several chain models were therefore tested. Alternating ferromagnetic/antiferromagnetic[34] and antiferromagnetic/antiferromagnetic[36] models would not reproduce the variable temperature magnetic data over the full temperature range. The Baker expression[38] (eqn. (3)), derived from a high temperature

$$\chi = \frac{N\beta^2 g^2}{4kT}\left(\frac{A}{B}\right)^{2/3} \quad (3)$$

$$A = 1.0 + 5.798x + 16.9027x^2 + 29.3769x^3 + 29.8329x^4 + 14.0369x^5$$

$$B = 1.0 + 2.798x + 7.0087x^2 + 8.6538x^3 + 4.5743x^4$$

$$x = J/2kT$$

series expansion and corrected for interchain coupling, provided a reasonable fit of the data, but did not reproduce the low temperature maximum in μ successfully ($g = 2.07$, $J = 13.6$ cm^{-1}, $zJ' = -3.9$ cm^{-1}, $\rho = 0.0001$, $N\alpha = 60 \times 10^{-6}$ cm^3 mol^{-1}, $10^2R = 1.5$). However it did successfully reproduce the low temperature drop in μ associated with the antiferromagnetic term and suggests the viability of a ferromagnetic chain model despite the irregular nature of the chains.

The very high moments at low temperature (2.14 μ_B at 14 K (**1**); 2.26 μ_B at 12 K (**2**)) suggest that it may be possible to associate an effective spin (S_{eff}) with the apparent ferromagnetic chains, and that each chain can be treated as a classical spin. $1/\chi$ *versus* temperature plots for **1** and **2** above 12 K have positive temperature intercepts (4.7 K (**1**), 6.9 K (**2**)), indicative of overall ferromagnetic behaviour. Magnetization *versus* field (0.1 to 5.0 T) data at 2 K for **1** and **2** fall well below the Brillouin curve for an $S = \frac{1}{2}$ species, while at 10 K and 20 K the magnetization data are in between the Brillouin curves typical of $S = \frac{1}{2}$ and $S = 1$ species. This suggests that the chains may be regarded as having classical spin behaviour. The classical spin model developed by Fischer,[39] corrected for interchain coupling (eqn. (4), (5)) was therefore used, and it provided an excellent

$$\chi_{chain} = Ng^2\beta^2S(S + 1)/3kT(1 + u)/(1 - u) \quad (4)$$

$$u = \coth(X) - \coth(1/X);\ X = JS(S + 1)/kT;\ S = \tfrac{1}{2}$$

$$\chi = \chi_{chain}/\{1 - \chi_{chain}(2zJ'/g^2N\beta^2)\} \quad (5)$$

fit of the data for both compounds over the full temperature range. This model assumes a single intra-chain J value (J) and an interchain exchange term (zJ'). The solid line in Fig. 8 illustrates the best data fit to the modified chain expression for **2** with $g = 2.106(5)$, $J = 9.9(2)$ cm^{-1}, $zJ' = -51.0$ (5) cm^{-1}, $\rho = 0.001$, $N\alpha = 60 \times 10^{-6}$ cm^3 mol^{-1} ($10^2R = 0.14$). A similar fit for **1** gave $g = 2.120(3)$, $J = 7.9(1)$ cm^{-1}, $zJ' = -56.0(4)$, $\rho = 0.001$, $N\alpha = 60 \times 10^{-6}$ cm^3 mol^{-1} ($10^2R = 0.2$). The fits required very large zJ' terms, indicating a very substantial interchain antiferromagnetic interaction. This would be consistent with the numerous inter-layer non-orthogonal associations identified in the structures (*vide ante*), and metamagnetic behaviour.

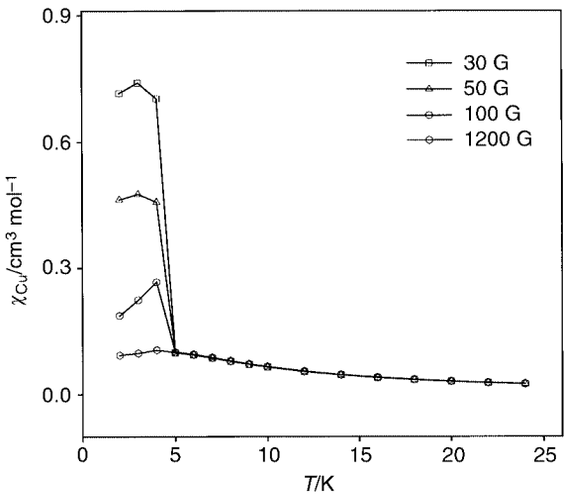

Fig. 9 Plot of χ_{Cu} at variable field for **2** in the temperature range 2–25 K.

An examination of the low field magnetization data for **1** and **2**, at low temperatures, revealed that magnetic susceptibility and magnetic moment rise slightly as the field is reduced below 0.1 T. On further reduction of the field a sharp discontinuity is observed at fields of 100 G or less. Fig. 9 illustrates a plot of χ_{Cu} against temperature for **2** at variable field, showing a pronounced increase in χ just below 5 K, which reaches a maximum at 3 K and ≈30 G. At fields of 1000 G and greater this feature is completely suppressed. A χT_{max} value of 2.8 cm^3 K mol^{-1} was observed for **2** at 4 K and 30 G. A similar result was found for **1**, with a sharp increase in χ below 4 K (χT_{max} 0.93 cm^3 K mol^{-1} at 3 K and 50 G). This surprising result suggests that in addition to the two exchange components identified at higher field, there must be a weak, extended ferromagnetic component as well, which shows up as a ferromagnetic phase transition in a weak field regime only ($T_c \approx 4$ K (**1**); $T_c \approx 5$ K (**2**)). This perhaps calls into question the inclusion of the low temperature magnetic data in the Fischer inter-chain analysis, despite the good data fit, but since substantially higher fields were used (0.1 T and greater), conditions under which the extended, weak ferromagnetic term appears to be suppressed, the analysis is reasonable. Magnetization data for **1** and **2** were examined at variable field, below T_c, and magnetic hysteresis behaviour was observed in both cases in the low field regime, confirming long range order, and molecular magnetic behaviour. Fig. 10 shows a plot of magnetization (cm^3 G mol^{-1}) *versus* field in the range 300 to −300 G for **2** at 4 K (coercive field 22 G; remanent magnetization 38 cm^3 G mol^{-1}). Complex **1** shows similar behavior with a coercive field of 17 G and a remanent magnetization of 46 cm^3 G mol^{-1} at 3 K. Pinpointing the origin of this extended effect is clearly difficult, but it may be associated with the close proximity of the 'ferromagnetic chains' within the two-dimensional sheets. Raising the temperature to 10 K in both cases destroyed the hysteresis curves. Complex **3** does not show any hysteretic behavior, as would be expected.

Complexes **1** and **2** therefore behave as molecular magnets below 4.0 K, which is an unusual feature for simple copper(II) complexes with structures based on simple repeating dinuclear subunits. The dramatic difference between the extended magnetic properties of **1** and **2**, and the much simpler magnetic properties of **3**, reflects a subtle structural difference between the two types of compound, which seems to be related, in large measure, to the presence of the water molecule in the structure in one case and not in the other. The magnetic properties of the parent compound of **3**, $[Cu_2(pahap)Cl_4]\cdot H_2O$, were investigated in an earlier study[20] using the Faraday technique at a field of 1.5 T, in the temperature range 4.0–300 K. The magnetic

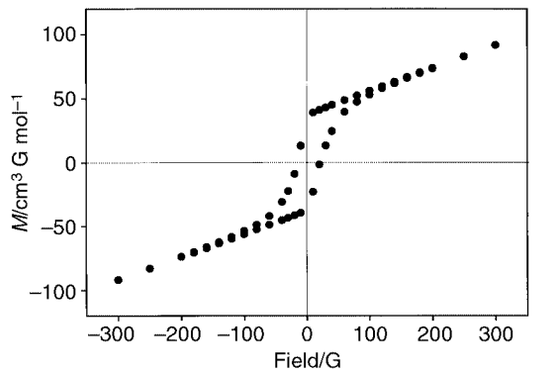

Fig. 10 Hysteresis plot for **2** at 4 K in the range −300 to 300 G.

moment increased from a value of 1.87 μ_B at 300 K to 1.98 μ_B at 15.9 K, and then dropped slightly to 1.71 μ_B at 4.0 K. These data were successfully fitted to eqn. (2), with $g = 2.14(1)$, $2J = 24.0(2)$ cm^{-1}, $\theta = -1.85$ K, $Na = 20 \times 10^{-6}$ cm^3 mol^{-1} ($10^2R = 1.3$). A repeat study using the SQUID technique at 0.5 T revealed similar behaviour and data fitting to eqn. (2) gave comparable parameters. The slight drop in moment at low temperature is indicative of the presence of an antiferromagnetic term, which would most reasonably be expected to be intermolecular in origin, but it is clearly very weak. Magnetization *versus* field (−200 to 200 G) data at 3 K showed no hysteresis.

Conclusion

Two nominally dinuclear complexes with copper(II) magnetic planes juxtaposed at acute angles about a N–N single bond have two-dimensional layer structures composed of interconnected chains, with significant associations between the layers. The magnetic structures of these compounds are best explained in terms of ferromagnetic linear chain arrangements, with extended antiferromagnetic coupling occurring between the layers of chains, *i.e.* metamagnetic behavior. Magnetic hysteresis is observed at 4.0 K and below, with small coercive fields and remanent magnetization, indicating an additional weak extended ferromagnetic component resulting in low temperature molecular magnetic behaviour. A related dinuclear complex exhibiting an extended linear chain structure with a much larger rotational angle between the copper magnetic planes around the N–N bond exhibits magnetic properties typical of a linear chain, but dominated by moderate intradinuclear antiferromagnetic exchange.

Acknowledgements

We thank the Natural Sciences and Engineering Council of Canada (NSERC), EPSRC (UK), and Monbusho (Japan) for financial support for this study.

References

1 Z. Xu, Ph.D. Thesis, Memorial University of Newfoundland, 1998.
2 (*a*) W. J. Stratton and D. H. Busch, *J. Am. Chem. Soc.*, 1960, **82**, 4834; (*b*) W. J. Stratton and D. H. Busch, *J. Am. Chem. Soc.*, 1958, **80**, 1286; (*c*) W. J. Stratton and D. H. Busch, *J. Am. Chem. Soc.*, 1958, **80**, 3191.
3 W. J. Stratton and P. J. Ogren, *Inorg. Chem.*, 1970, **9**, 2588.
4 P. D. W. Boyd, M. Gerloch and G. M. Sheldrick, *J. Chem. Soc., Dalton Trans.*, 1974, 1097.
5 J. Saroja, V. Manivannan, P. Chakraborty and S. Pal, *Inorg. Chem.*, 1995, **34**, 3099.
6 C. J. O'Connor, R. J. Romananch, D. M. Robertson, E. E. Eduok and F. R. Fronczek, *Inorg. Chem.*, 1983, **22**, 449.
7 T. C. Woon, L. K. Thompson and P. Robichaud, *Inorg. Chim. Acta*, 1984, **90**, 201.
8 P. Souza, A. I. Matesanz and V. Fernández, *J. Chem. Soc., Dalton Trans.*, 1996, 3011.
9 J. García-Jojal, J. García-Jaca, R. Cortés, T. Rojo, M. K. Urtiaga and M. I. Arriortua, *Inorg. Chim. Acta*, 1996, **249**, 25.
10 A. Mangia, C. Pelizzi and G. Pelizzi, *Acta Crystallogr., Sect. B*, 1974, **30**, 2146.
11 A. Bonardi, S. Ianelli, C. Pelizzi and G. Pelizzi, *Inorg. Chim. Acta,* 1991, **187**, 167.
12 A. Bacchi, A. Bonini, M. Carcelli, F. Ferraro, E. Leporati, C. Pelizzi and G. Pelizzi, *J. Chem. Soc., Dalton Trans.*, 1996, 2699.
13 A. E. Koziol, R. C. Palenik and G. J. Palenik, *J. Chem. Soc., Chem. Commun.*, 1989, 650.
14 M. Lagrenée, S. Sueur and J. P. Wignacourt, *Acta Crystallogr., Sect. C*, 1991, **47**, 1158.
15 A. Bacchi, L. P. Battaglia, M. Carcelli, C. Pelizzi, G. Pelizzi, C. Solinas and M. A. Zoroddu, *J. Chem. Soc., Dalton Trans.*, 1993, 775.
16 E. W. Ainscough, A. M. Brodie, J. D. Ranford and J. M. Waters, *Inorg. Chim. Acta*, 1995, **236**, 83.
17 X. Chen, S. Zhan, C. Hu, Q. Meng and Y. Liu, *J. Chem. Soc., Dalton Trans.*, 1997, 245.
18 P. J. van Koningsbruggen, E. Muller, J. G. Haasnoot and J. Reedijk, *Inorg. Chim. Acta*, 1993, **208**, 37.
19 C. J. Matthews, K. Avery, Z. Xu, L. K. Thompson, L. Zhao, D. O. Miller, K. Biradha, K. Poirier, M. J. Zaworotko, C. Wilson, A. E. Goeta and J. A. K. Howard, *Inorg. Chem.*, 1999, **38**, 5266.
20 Z. Xu, L. K. Thompson and D. O. Miller, *Inorg. Chem.*, 1997, **36**, 3985.
21 L. K. Thompson, Z. Xu, A. E. Goeta, J. A. K. Howard, H. J. Clase and D. O Miller, *Inorg. Chem.*, 1998, **37**, 3217.
22 Z. Xu, L. K. Thompson, C. J. Matthews, D. O. Miller, A. E. Goeta, C. Wilson, J. A. K. Howard, M. Ohba and H. Ōkawa, *J. Chem. Soc., Dalton Trans*, 2000, 69.
23 D. S. Brown, V. H. Crawford, J. W. Hall and W. E. Hatfield, *J. Phys. Chem.*, 1977, **81**, 1303.
24 A. Altomare, M. Cascarano, C. Giacovazzo and A. Guagliardi, SIR92, *J. Appl. Crystallogr.*, 1993, **26**, 343.
25 P. T. Beurskens, G. Admiraal, G. Beurskens, W. P. Bosman, R. de Gelder, R. Israel and J. M. M. Smits, DIRDIF94, The DIRDIF-94 program system, Technical Report of the Crystallography Laboratory, University of Nijmegen, 1994.
26 D. T. Cromer and J. T. Waber, *International Tables for X-ray Crystallography*, The Kynoch Press, Birmingham, 1974, vol. IV, Table 2.2 A.
27 J. A. Ibers and W. C. Hamilton, *Acta Crystallogr.*, 1964, **17**, 781.
28 D. C. Creagh and W. J. McAuley, *International Tables for Crystallography*, ed. A. J. C. Wilson, Kluwer Academic Publishers, Boston, 1992, vol. C, Table 4.2.6.8, pp. 219–222.
29 teXsan for Windows, Crystal Structure Analysis Package, Molecular Structure Corporation, Houston, TX, 1997.
30 J. Cosier and A. M. Glazer, *J. Appl. Crystallogr.*, 1986, **19**, 105.
31 (*a*) SMART Data Collection Software, version 4.050, Siemens Analytical X-ray Instruments Inc., Madison, WI, 1996; (*b*) SAINT Data Reduction Software, version 4.050, Siemens Analytical X-ray Instruments Inc., Madison, WI, 1996.
32 G. M. Sheldrick, SHELXTL 5.04/VMS, An integrated system for solving, refining and displaying crystal structures from diffraction data, Siemens Analytical X-ray Instruments Inc., Madison, WI, 1995.
33 A. R. Katritzky and A. R. Hands, *J. Chem. Soc.*, 1958, 2202.
34 J. J. Borrás-Almenar, E. Coronado, J. Curely, R. Georges and J. C. Gianduzzo, *Inorg. Chem.*, 1994, **33**, 5171.
35 B. Bleaney and K. D. Bowers, *Proc. R. Soc. London, A*, 1952, **214**, 451.
36 J. W. Hall, W. E. Marsh, R. R. Weller and W. E Hatfield, *Inorg. Chem.*, 1981, **20**, 1033.
37 L. K. Thompson, S. S. Tandon, F. Lloret and M. Julve, *Inorg. Chem.*, 1997, **36**, 3301.
38 G. A. Baker and G. S. Rushbrooke, *Phys. Rev.*, 1964, **135**, 1272.
39 M. E. Fischer, *Am. J. Phys.*, 1964, **32**, 343.